Experimental verification of dose enhancement effects in a lung phantom from inline magnetic fields

Bradley M. Oborn[a,b], Maegan A. Gargett[c,b], Trent J. Causer[a,b], Sarah J. Alnaghy[b,e], Nicholas Hardcastle[d,b], Peter E. Metcalfe[b,e], Paul J. Keall[f,e]

[a] Illawarra Cancer Care Centre, Wollongong, Australia
[b] Centre for Medical Radiation Physics, University of Wollongong, Australia
[c] Northern Sydney Cancer Centre, St Leonards, Australia
[d] Peter MacCallum Cancer Centre, Melbourne, Australia
[e] Ingham Institute for Applied Medical Research, Liverpool, Australia
[f] Sydney Medical School, University of Sydney, Australia

Conflict of interest statement

The authors have no conflicts of interest to disclose.

Abstract

Background and purpose

To present experimental evidence of lung dose enhancement effects caused by strong inline magnetic fields.

Materials and methods

A permanent magnet device was utilised to generate 0.95 T–1.2 T magnetic fields that encompassed two small lung-equivalent phantoms of density 0.3 g/cm^3. Small 6MV and 10MV photon beams were incident parallel with the magnetic field direction and Gafchromic EBT3 film was placed inside the lung phantoms, perpendicular to the beam (experiment 1) and parallel to the beam (experiment 2). Monte Carlo simulations of experiment 1 were also performed.

Results

Experiment 1: The 1.2 T inline magnetic field induced a 12% (6MV) and 14% (10MV) increase in the dose at the phantom centre. The Monte Carlo modelling matched well (±2%) to the experimentally observed results. Experiment 2: A 0.95 T field peaked at the phantom centroid (but not at the phantom entry/exit regions) details a clear dose increase due to the magnetic field of up to 25%.

Conclusions

This experimental work has demonstrated how strong inline magnetic fields act to enhance the dose to lower density mediums such as lung tissue. Clinically, such scenarios will arise in inline MRI-linac systems for treatment of small lung tumours.

Introduction

Real-time MRI-guided radiotherapy treatments have been delivered for over two years through the ViewRay system [1]. Patient treatments on the Unity 1.5 T MRI-linac system are planned before the end of 2017 [2]. In both of these systems the magnetic field of the MRI scanner is perpendicular to the X-ray beam direction. This leads to various dose changes, with respect to the no magnetic field case, that need addressing such as the electron return effect (ERE) [3]. In terms of basic dose planning calculation quantities, a transverse magnetic field sets up an asymmetric tilting of the secondary electron dose kernel due to the Lorentz force. This tilting becomes stronger as magnetic field strength increases [4], and the ERE can be considered as an artefact of this process that occurs at boundaries between different density mediums. Recent modelling work has shown successfully however that these effects, with appropriate planning, should be negligible in the Unity system for lung stereotactic body radiotherapy treatments [5].

In two other non-clinical prototype MRI-linac systems, the Aurora-RT [6], and the Australian MRI-linac [7], the magnetic field is parallel or inline with the X-ray beam direction. In these two prototype systems it could be expected that the inline orientation design was envisaged as a solution to the ERE. To be more specific, in this orientation the magnetic field acts to slightly lengthen the dose kernel in the forward direction. In water, this leads to very minimal differences between 1 T and 0 T. However in much lower density mediums such as lung, there is a stronger stretching of the dose kernel in the forward direction. This also narrows the width of the dose kernel, and so sets up a small increase in intensity in the forward direction. Basic superposition of these kernels, to estimate the dose from a small X-ray beam, will result in beams with narrower penumbral widths and slightly stronger doses. The concept of generating a more conformal dose distribution by applying inline magnetic fields has been investigated previously for X-ray beams in water phantoms using both simulations and experiments [8], [9], [10]. The first basic simulation work however on changes in lung tissue doses due to inline magnetic fields was reported in 2010 [11]. More recent work studied the impact of a 1 T inline magnetic field on 8 clinical small lung tumour cases planned with 6MV 3D-CRT treatments [12]. A compelling prediction of this modelling work was that the mean dose to the PTV could be enhanced by as much as 22% when the magnetic field was included, for small lung tumours around <3 cc in volume. We do note however a high skin dose induced in the Australian MRI-linac system [13], [14], which is not reported in the Aurora-RT system [15]. In general, the advantages of the inline systems over the perpendicular systems is the improved patient dosimetry (no ERE), however this comes at the cost of rotating the magnet around the patient (Aurora-RT) or rotating the patient (Australian MRI-linac). For a more in-depth summary of the benefits and disadvantages of the various MRI-linac systems we refer the reader to Table 2 in Keall et al. [7].

In this work, we report experimental evidence of the dose changes observed in a lung phantom when surrounded by strong inline magnetic fields of 0.95 T–1.2 T.

Materials and methods

Permanent magnet system

A portable permanent magnet based system was used to generate a strong magnetic field over a small volume. This system is shown in Fig. 1. Two banks of NdFeB permanent magnets are held in a steel yoke with focusing cones to concentrate the magnetic flux across the pole gap. Holes of 5×5 cm^2 in cross-section in the magnet banks and steel yoke allowed for the X-ray beam to be incident inline with the magnetic field. The two experimental setups are shown in Fig. 1. In experiment 1, a 3 cm gap between the cone tips exists and the magnetic field generated directly across the gap is peaked at 1.2 T. In this case, the 6 cm thick steel cone tips contain a 0.5 cm wide split along the central axis to allow the radiation beam to pass through.

In experiment 2, the cone tip gap is also 3 cm however a 2.5×2.5 cm^2 hole exists in the middle of the cones. This allows for X-ray beams of 2×2 cm^2 to pass through the device uninterrupted. The magnetic field generated across the gap is peaked at 0.95 T.

Phantom setup and film measurements

Phantom 1 consisted of a 7.5×5 cm^2 piece of Gafchromic EBT3 film sandwiched between two pieces of lung equivalent phantom. The two phantom pieces were $5 \times 7.5 \times 2$ cm^3 and $5 \times 7.5 \times 1$ cm^3 in size. Phantom two consisted of a 15×2.4 cm^2 piece of EBT3 film sandwiched between two lung phantoms blocks of size $1.2 \times 2.4 \times 15$ cm^3.

The EBT3 films were calibrated following the methods outlined by Devic et al. [16] using a standard single-channel analysis procedure (red channel) to convert net optical density to dose, for a dose range of 0–5 Gy. Films were scanned on an EPSON (10000XL) flatbed scanner with 150 dpi resolution. The average of 3 scans were used for analysis. The estimated standard uncertainty associated with these measurements is ± 3%.

Phantom irradiation with magnetic field

The magnet device was positioned such that the source to magnet isocenter was 150 cm for all measurements. This distance is designed to approximately match the source-to-isocenter distance (SID) of the Australian MRI-linac system [14]. The fringe field of the magnet was measured to be <2 Gauss at 1 m from isocenter and so deemed not to have any impact on the output of the Linac (Varian Clinac 2100C). 6MV and 10MV beams of field size (at 150 cm SID) 3×3 cm^2 (experiment 1) and 1.4×1.4 cm^2 and 2.0×2.0 cm^2 (experiment 2) were delivered to the lung phantoms.

Phantom irradiation without magnetic field

All experiments performed within the magnet were repeated without the magnetic field. In these reference zero-field conditions, the same focusing cones were used to hold the phantoms in a replica arrangement. The steel focusing cones were held in the same position as the in-magnet positions using an aluminium frame. Hence the entire steel circuit is not present but only the important steel surrounding the phantom. This ensures that the identical scattering conditions surrounding the phantoms are preserved when compared with the case that included the magnetic field.

Monte Carlo simulation

Geant4 version 10.1 was used to simulate the experiment 1 setup as an independent cross-check of the results observed with film (Fig. 2). In this simulation the X-ray beam was modelled from reading phase space files of matching small fields. These were generated using an existing in-house Monte Carlo system that has been benchmarked and reported elsewhere [17]. Geometry was setup that matched the permanent magnet device, and a full 3D magnetic field map was introduced into the simulation. This was generated by finite element modelling (COMSOL), and the volume encompassed included the entire magnet device. Thus particle tracking considers an accurate representation of the experimental setup and surrounding magnetic field. Dose was scored in a volume that matched the film shape and location. The virtual film pixel resolution was 1×1 mm, and the film thickness was modelled as being 0.25 mm. For each simulation a total of 1×10^8 particles were fired from the phase space (94.2 cm above isocenter of the magnet). 10 parallel simulations were run and the results merged to produce a standard error in the virtual film pixels of around ± 2%.

Results

Experiment 1

Fig. 3, Fig. 4 display a summary of the films taken in experiment 1 for the 6MV and 10MV beams respectively. On the left we see the calibrated film results and on the right we see the Monte Carlo equivalent films. In the middle profiles are presented through the beam in the short axis. The beam width in this case is only 0.5 cm wide, and is a result of beam transmission through the 0.5 cm gap in the steel focusing cone tips. These tips are 6 cm in thickness and so there is partial transmission of the beam, as seen by the lateral profile dose off-axis being around 30% of the open field dose. A 3×3 cm^2 beam was incident down the portal which passed through the cone tips. This 3×3 cm^2 beam outline is clearly evident in the film images. For the 6MV beam the inline magnetic field of 1.2 T clearly acts to enhance the dose within the beam area, or the order of 12%. At 0.5 cm from the beam central axis the enhancement appears minimal as the profiles start to align. For the 10MV beam there is a slightly stronger enhancement within the beam area, i.e. 14%. The biggest difference however is the stronger dose enhancement off-axis. The B = 0 T profiles align with the B = 1.2 T profiles only at about 1.5 cm from the beam central axis.

Experiment 2

Fig. 5 displays the result of experiment 2. On the left are the results for the beams. The right side shows the 10MV data. The film is also presented at the top for the B = 0.95 T case and the two beam field sizes are shown. A central axis percentage-depth-dose profile is extracted from the two cases and shown in the middle profile plots, along with the magnetic field strength along the beam central axis. The magnetic field at the start and end of the phantom is essentially zero in field strength due to coinciding with the hole in the focusing cones and steel yoke. The first and most obvious feature of these films is the clear central axis dose increases that occurs directly where the inline magnetic field is strongest. In the strongest regions of enhancement, namely from 7 cm to 7.5 cm depth along the phantom, the relative dose enhancement is in the order of 15% (6MV, 1.4×1.4 cm^2 beam), 18% (6MV, 2.0×2.0 cm^2 beam), 20% (10MV, 1.4×1.4 cm^2

beam), and 25% (10MV, 2.0×2.0 cm^2 beam). Furthermore, the central axis PDD profiles align very well at the start and end of the phantoms, corresponding to where the magnetic field is zero in both the reference measurement and the with-magnet measurement.

Discussion

Experiment 1

In experiment 1 a shallow depth lung phantom was irradiated and film positioned at 2 cm depth. At this depth there is still some dose build-up occurring in lower density lung (as compared with water D_{max} being 1.5 cm and 2.1 cm for 6MV and 10MV respectively). Thus the results cannot be extrapolated to predict a full estimate of how the dose changes inside lung material when in strong inline magnetic fields. The experiment does however offer a full 2D plane of the dose change at this depth, where the profiles then are helpful to detail the dose changes off-axis, or outside the X-ray beam. In this experiment there is clearly a stronger and more broad off-axis dose enhancement effect for 10MV over 6MV. This can be seen in the profiles at 0.5 cm from the field edge, i.e. 7.5 mm from the CAX. In the 6MV beam almost no changes occur at this level with the magnetic field. At 10MV there is around 7–8% dose increase. This arises for two reasons: (1) the length of the dose kernel in lung for 10MV is significantly longer than for 6MV, i.e. based on scaling of dose kernels in water [18]. (2) the penetration of the 10MV beam through the 6 cm of steel cone tip is greater than the 6MV beam. Thus overall, there are more secondary electrons with longer ranges in the out-of-field region in the 10MV case.

Experiment 2

Experiment 2 presents a full dose build up in lung phantom along the central axis depth profile. This setup is designed to assist in the interpretation of the results from experiment 1. The magnetic field is also variable and is essentially zero at the start and ends of the phantom. This is due to the almost zero magnetic flux inside the beam portal area of the cones, i.e. there is no steel so minimal flux will pass through there. This unique magnetic field distribution and phantom arrangement allows us to see the impact of the magnetic field under charged particle equilibrium along the depth direction. The alignment of the profiles presented at the start and end of the phantom (for no-magnet vs with-magnet) shows the clear equivalence of the doses, but enhancement where the magnetic field increases. As expected, the overall maximum dose enhancement occurs at around the location of the peak of the magnetic field strength. The overall maximum enhancement value in experiment 2 is stronger than that shown in experiment 1, being as much as 25% for the 10MV 2.0×2.0 cm^2 beam. It is difficult to compare directly the results from experiment 1 and experiment 2. Experiment 1 has a wide phantom with good lateral direction charged particle equilibrium. Experiment 2 has good longitudinal direction charged particle equilibrium. In any case, previous works have detailed the expected dose changes at 1 T inline magnetic field in full scale, clinical lung plans [12]. A similar enhancement effect was predicted that can be utilized with multiple beams to boost dose to the PTV with minimal change to the surrounding healthy tissue.

Conclusion

X-ray beam dose changes in magnetic fields have been studied both experimentally and through simulations for several decades. The effects generated in transverse magnetic fields is well understood and verified. However for inline magnetic fields the dose changes have been less studied. In this work we have examined the changes induced in small X-ray beams in lung phantoms whilst exposed to magnetic fields around 1 T in strength and aligned parallel with the X-ray beam direction. The results clearly demonstrate how a strong inline magnetic field results in a local dose enhancement effect. The inline magnetic field encourages secondary electrons to travel in a more forwardly direction, resulting in a reduction of lateral secondary electron scattering in the lung medium. To the best of our knowledge, this experimental work presents for the first time evidence of the unique dose changes that occur in lung equivalent mediums when exposed to strong inline magnetic fields. This work directly strengthens the predictions of recent work describing the positive dose enhancement effects to the PTV in small lung tumour plans when treated with 6MV x-ray beams [12]. Such a result is an exciting element to bring to pre-clinical inline MRI-linac systems currently being developed. These systems ideally will offer the most superior soft tissue delineation of lung tumours in real-time. Coupled with a unique and positive, magnetically induced dose change, one could envisage that future inline MRI-linac based treatments will offer a significant improvement in both the quality and outcome of X-ray radiotherapy of lung tumour treatments over current methods.

References

[1] Mutic Sasa, Dempsey James F. The viewray system: magnetic resonance – guided and controlled radiotherapy. Semin Radiat Oncol 2014;24:196–9.

[2] Lagendijk Jan JW, Raaymakers Bas W, van Vulpen Marco. The magnetic resonance imaging-linac system. Semin Radiat Oncol 2014;24:207–9.

[3] Raaijmakers AJE, Raaymakers BW, Lagendijk JJW. Integrating a MRI scanner with a 6 MV radiotherapy accelerator: dose increase at tissue-air interfaces in a lateral magnetic field due to returning electrons. Phys Med Biol 2005;50:1363–76.

[4] Raaijmakers AJE, Raaymakers BW, Lagendijk JJW. Magnetic-field-induced dose effects in MR-guided radiotherapy systems: dependence on the magnetic field strength. Phys Med Biol 2008;53:909–23.

[5] Menten Martin J, Fast Martin F, Nill Simeon, Kamerling Cornelis P, McDonald Fiona, Oelfke Uwe. Lung stereotactic body radiotherapy with an mr-linac quantifying the impact of the magnetic field and real-time tumor tracking. Radiother Oncol 2016;119:461–6.

[6] Fallone Biagio Gino. The rotating biplanar linac – magnetic resonance imaging system. Semin Radiat Oncol 2014;24:200–2.

[7] Keall Paul J, Barton Michael, Crozier Stuart. The Australian magnetic resonance imaging – linac program. Semin Radiat Oncol 2014;24:203–6.

[8] Bielajew AF. The effect of strong longitudinal magnetic fields on dose deposition from electron and photon beams. Med Phys 1993;20:1171–9.

[9] Litzenberg DW, Fraass BA, McShan DL, O'Donnel TW, Roberts DA, Becchetti FD, et al. An apparatus for applying strong longitudinal magnetic fields to clinical photon and electron beams. Phys Med Biol 2001;46:N105–115.

[10] Chen Yu, Bielajew Alex F, Litzenberg Dale W, Moran Jean M, Becchetti Frederick D. Magnetic confinement of electron and photon radiotherapy dose: a Monte Carlo simulation with a nonuniform longitudinal magnetic field. Med Phys 2005;32:3810–8.

[11] Kirkby C, Murray B, Rathee S, Fallone BG. Lung dosimetry in a linac-MRI radiotherapy unit with a longitudinal magnetic field. Med Phys 2010;37:4722–32.

[12] Oborn BM, Ge Y, Hardcastle N, Metcalfe PE, Keall PJ. Dose enhancement in radiotherapy of small lung tumors using inline magnetic fields: a Monte Carlo based planning study. Med Phys 2016;43:368–77.

[13] Oborn BM, Kolling S, Metcalfe PE, Crozier S, Litzenberg DW, Keall PJ. Electron contamination modeling and reduction in a 1 T open bore inline MRI-linac system. 051708. Med Phys 2014;41:051708 [15p].

[14] Liney GP, Dong B, Begg J, Vial P, Zhang K, Lee F, et al. Technical note: experimental results from a prototype high-field inline mri-linac. Med Phys 2016;43:5188–94.

[15] Keyvanloo A, Burke B, Aubin JSt, Baillie D, Wachowicz K, Warkentin S, et al. Minimal skin dose increase in longitudinal rotating biplanar linac-mr systems: examination of radiation energy and flattening filter design. Phys Med Biol 2016;61:3527.

[16] Devic Slobodan, Seuntjens Jan, Sham Edwin, Podgorsak Ervin B, Ross Schmidtlein C, Kirov Assen S, et al. Precise radiochromic film dosimetry using a flat-bed document scanner. Med Phys 2005;32:2245–53.

[17] Oborn BM, Williams M, Bailey M, Carolan MG. IMRT treatment monitor unit verification using absolute calibrated BEAMnrc and Geant4 Monte Carlo simulations. J Phys: Conf Ser 2014;489:012020.

[18] Ahnesjo A, Andreo P. Determination of effective bremsstralung spectra and electron contamination for photon dose calculations. Phys Med Biol 1989;34:1451–64.

Fig. 1. Experimental setup. Left: experiment 1 contains a $5 \times 7.5 \times 3$ cm^3 lung phantom with film insert. Right: Experiment 2 contains a $2.4 \times 2.4 \times 15$ cm^3 lung phantom with film placed along the beam central axis and inside the cone tip holes. An outline of the lung phantom is shown superimposed.
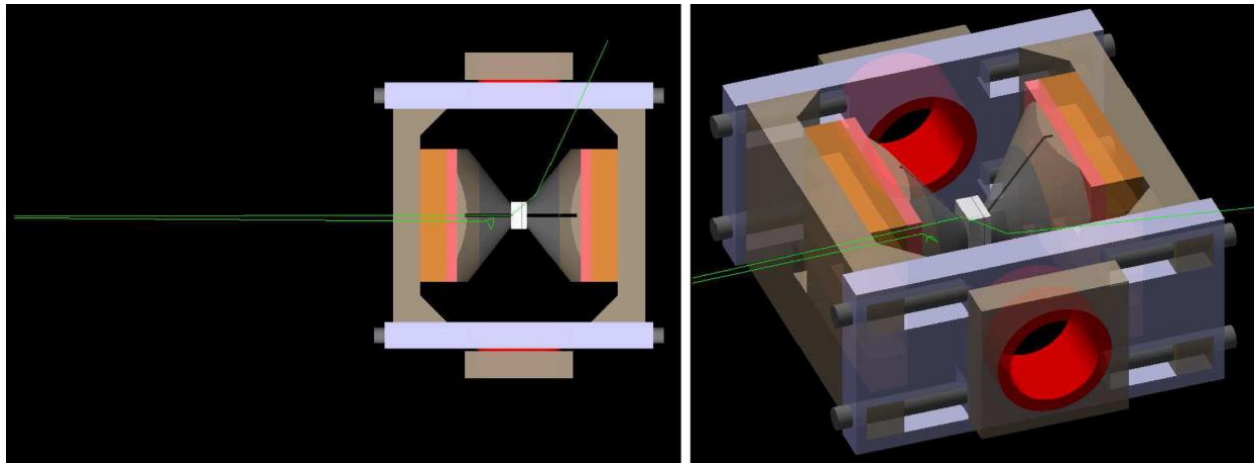
Fig. 2. Monte Carlo's setup of experiment 1. Left: a topview showing where the particles start from a phase space file positioned at 94.2 cm from the magnet isocentre. This equates to a SID of 150 cm. Right: 3D view of the Monte Carlo setup. In this view the portal in the steel yoke is shown to allow the beam to pass through to the phantom.
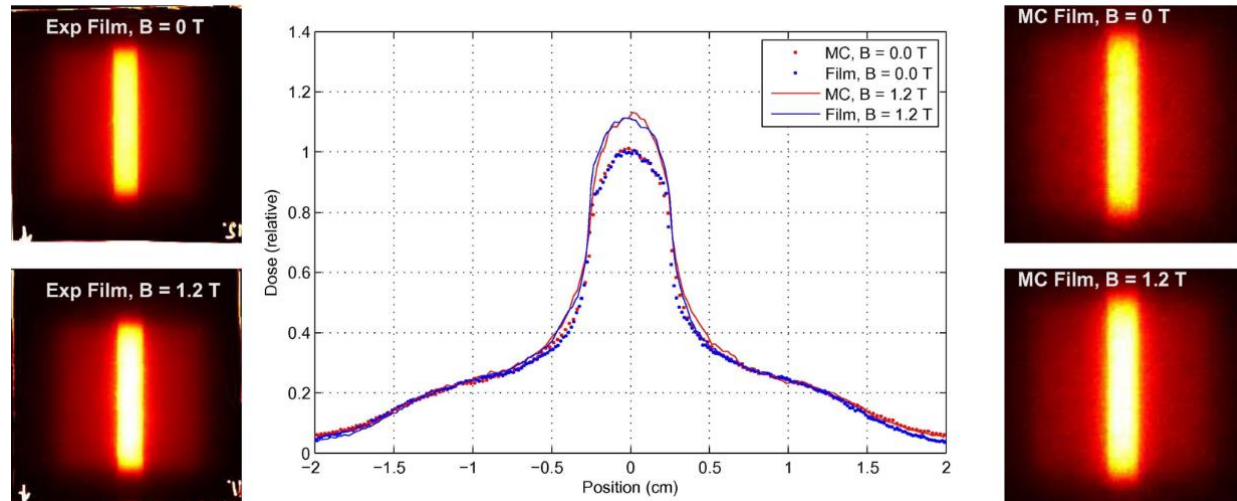
Fig. 3. Films and profile results for the 1.2 T field, 0.5×3 cm² beams at energy of 6MV. On the left the experimental films are presented. On the right the Monte Carlo films are displayed. In the middle profiles are presented through the short axis of the beam cross-section. A clear dose enhancement of around 12% is observed when the magnetic field is applied. The 3×3 cm² partial beam transmission is also clearly observed in each of the film inserts.
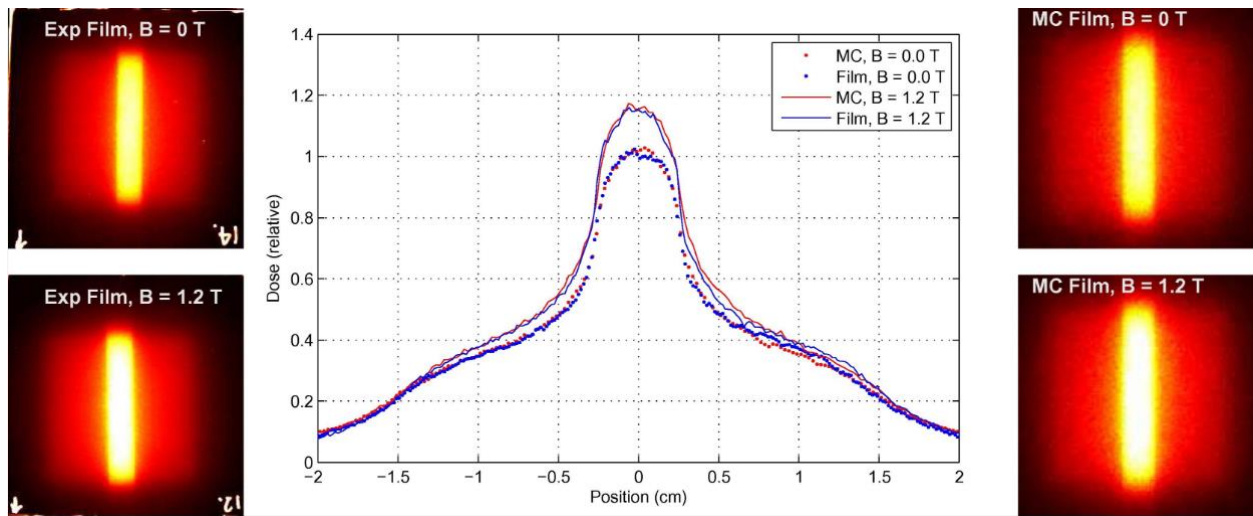
Fig. 4. Films and profile results for the 1.2 T field, 0.5×3 cm^2 beams at energy of 10MV. On the left the experimental films are presented. On the right the Monte Carlo films are displayed. In the middle profiles are presented through the short axis of the beam cross-section. A clear dose enhancement of around 14% is observed when the magnetic field is applied. The 3×3 cm^2 partial beam transmission is also clearly observed in each of the film inserts.
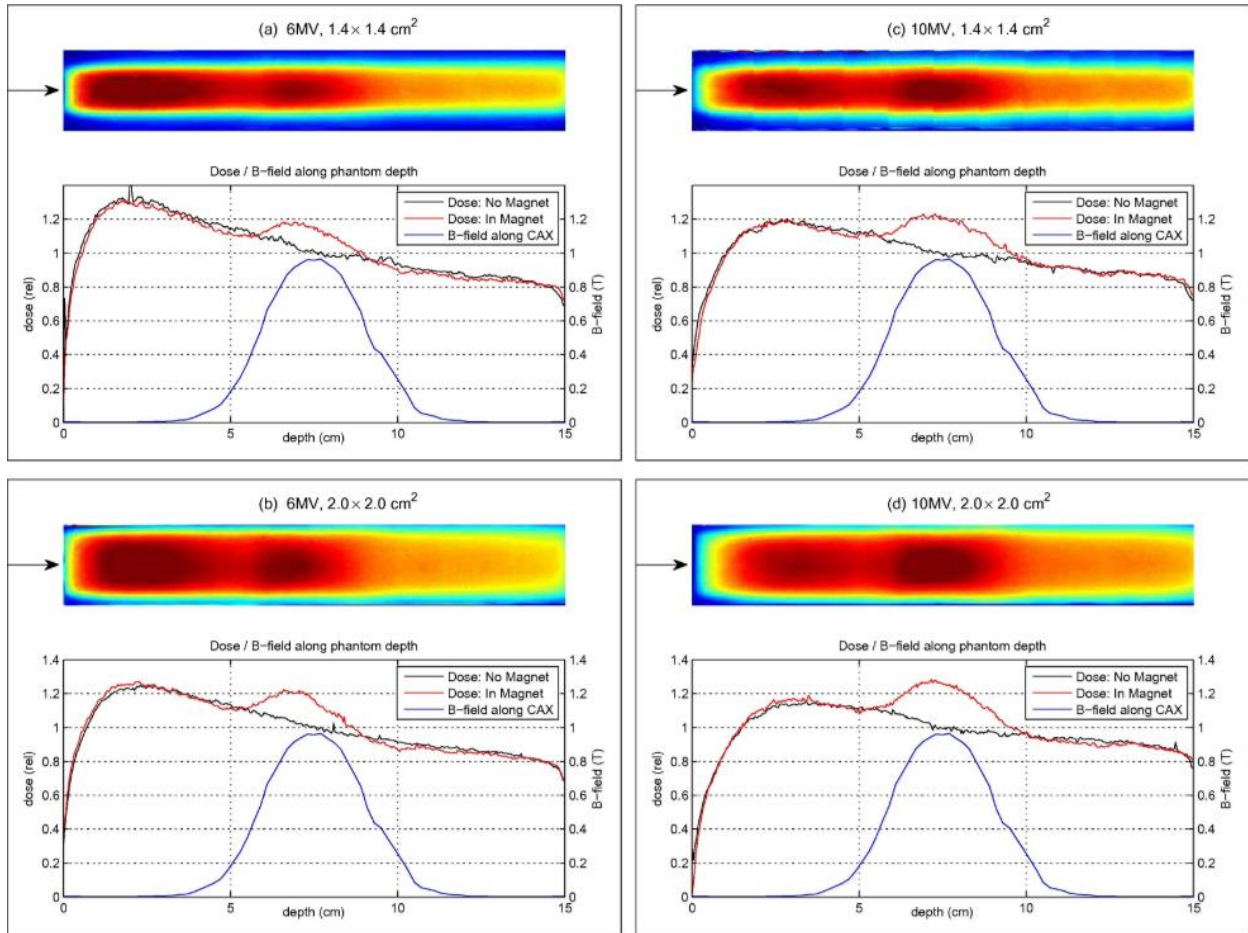
Fig. 5. Results of the films recorded in experiment 2. (a) 6MV at 1.4×1.4 cm^2 field size. (b) 6MV at 2.0×2.0 cm^2 size. (c) 10MV at 1.4×1.4 cm^2 field size. (d) 10MV at 2.0×2.0 cm^2 field size. In each part the film recorded in the with-magnet experiment is displayed on the top. On the bottom central axis depth-dose profiles are shown which compare directly the no-magnet to with-magnet results. The dose is normalised to the no-magnet experiment at the phantom centroid. The right axis displays the magnetic field strength along the depth of the phantom for the with-magnet setup. For all with-magnet experiments a clear increase in dose is observed which is related directly to the location and strength of the inline magnetic field surrounding the phantom.